Behavioral/Systems/Cognitive

Behavioral State Modulates the Activity of Brainstem Sensorimotor Neurons

Kimberly L. McArthur and J. David Dickman
Department of Anatomy & Neurobiology, Washington University School of Medicine, St. Louis, Missouri 63110

Sensorimotor processing must be modulated according to the animal's behavioral state. A previous study demonstrated that motion responses were strongly state dependent in birds. Vestibular eye and head responses were significantly larger and more compensatory during simulated flight, and a flight-specific vestibular tail response was also characterized. In the current study, we investigated the neural substrates for these state-dependent vestibular behaviors by recording extracellularly from neurons in the vestibular nuclear complex and comparing their spontaneous activity and sensory responses during default and simulated flight states. We show that motion-sensitive neurons in the lateral vestibular nucleus are state dependent. Some neurons increased their spontaneous firing rates during flight, though their increased excitability was not reflected in higher sensory gains. However, other neurons exhibited state-dependent gating of sensory inputs, responding to rotational stimuli only during flight. These results demonstrate that vestibular processing in the brainstem is state dependent and lay the foundation for future studies to investigate the synaptic mechanisms responsible for these modifications.

Introduction

Sensorimotor processing can be strongly modified by the animal's behavioral state. Even reflex circuits may be optimized for different environmental, physiological, or motivational conditions. Sensory cues repeatedly associated with these conditions then evoke retrieval of the optimal sensorimotor mappings for a particular state. For example, gliding flight is a distinct behavioral state in pigeons that can be simulated in the laboratory with frontal airflow (Bilo and Bilo, 1978, 1983; Bilo, 1992, 1994; Gioanni and Sansonetti, 1999, 2000; Maurice and Gioanni, 2004a,b). During flight, active gaze and posture stabilization are critical, as turbulence threatens perception and performance (Brown, 1963; Erichsen et al., 1989; Warrick et al., 2002). This is reflected in state-dependent vestibular gaze-and posture-stabilizing responses (McArthur and Dickman, 2011). Eye [vestibulo-ocular (VOR)] and head [vestibulocollic (VCR)] responses to rotation had significantly higher gains during simulated flight. Also, state-specific vestibular tail reflexes were observed that would contribute to postural stability during flight.

What is the neural substrate of these state-dependent behaviors? Two questions must be addressed: which neurons in the underlying sensorimotor pathways are state dependent, and which features of the neural response are likely to drive the observed changes in behavior? Vestibular reflexes are generated in part by a three-neuron arc, wherein vestibular afferents project to brainstem neurons in the vestibular nuclear complex (VNC), which in turn project to motor nuclei (Precht, 1979; Wilson and Peterson, 1981). Modulations of vestibular behaviors may be reflected in the responses of VNC neurons, as observed for floccular target neurons following VOR adaptation (Lisberger et al., 1994) and position-vestibular-pause neurons during VOR suppression (Cullen et al., 1993; Roy and Cullen, 2002). VNC neurons may also incorporate the context of stimulation into their responses, as when neurons suppress responses to active head movements (McCrea et al., 1999; Roy and Cullen, 2004). Further, Rabin (1973, 1974, 1975a,b) demonstrated in pigeons that vestibular projections to the spinal cord—but not labyrinthine inputs to the brainstem—were active in the absence of airflow, suggesting state-specific gating or facilitation of vestibular afferent signals to central vestibular neurons. Here, we examined the neural substrate of state-dependent vestibular reflexes by recording from lateral vestibular nucleus (LVN) cells, known to be a strong source of vestibulospinal projections involved in head and tail responses (Wilson and Peterson, 1981). We anticipated that state dependence would be reflected in the gain of firing rate modulations to sinusoidal motion. Since both eye and head reflexes were active across states but had higher gains during flight, we predicted that a subset of VNC neurons would likewise be motion sensitive across states but would increase their gains during flight. To drive flight-specific tail reflexes, we predicted that another subset of VNC neurons would exhibit flight-specific motion sensitivity, with gains equal to zero during the default state. We present data suggesting that behavioral state does modulate VNC neuronal excitability, reflected in the sensory gains of some neurons and in the overall spiking activity of others.

Received Feb. 17, 2011; revised July 5, 2011; accepted Aug. 17, 2011.

Author contributions: K.L.M. and J.D.D. designed research; K.L.M. performed research; K.L.M. analyzed data; K.L.M. and J.D.D. wrote the paper.

This work was supported in part by National Institutes of Health Grants DC-010373, DC-007618, DC-006913, and DC-009734. The authors thank Kathleen M. Reed, Casey Carroll, and Candace Ward for expert assistance with brain tissue processing. We thank Dr. Jeffrey Taube and his laboratory for instruction and advice in the implementation of the chronically implanted microdrive. Finally, We thank Dr. Dora E. Angelaki for insight and suggestions regarding data analysis and presentation.

Correspondence should be addressed to Dr. J. David Dickman at his present address: Department of Neuroscience, One Baylor Plaza, Mail Stop BCM295, Baylor College of Medicine, Houston, TX 77030. E-mail: dickman@bcm.edu.

DOI:10.1523/JNEUROSCI.0891-11.2011

 0270-6474/11/3116700-09$15.00/0

Materials and Methods

Four adult pigeons (*Columba livia*) of both sexes, ranging in weight from 400 to 700 g, were used in accordance with the guidelines set forth by the National Institutes of Health *Guide for the Care and Use of Animals in Research*, as well as those approved by the Institutional Animal Care and Use Committee. The animals were housed and cared for in the Laboratory Animal Facilities under veterinary supervision.

Animal preparation. The neural recording assembly (Kubie, 1984; Taube et al., 1990) consisted of a custom chronic microdrive with an array of 10 electrodes. The electrode array was constructed of 25 μm insulated nichrome wires (60% Ni/16% Cr/24% Fe, California Fine Wire) encased in a stainless steel cannula. The wires were connected to a modified circular connector (10-pin circular transistor socket, Mill-Max) encased in dental acrylic with three drive screws, each of which was partially threaded into a tapped nylon cuff. Each animal was surgically implanted with one of these recording assemblies under isofluorane anesthesia (3–5% in O_2 via endotracheal intubation). Both heart rate (80–150 beats/min) and core temperature (40°C) were monitored and maintained throughout surgery. The animal's head was secured in a stereotaxic device. An incision was made along the midline of the skull, and the underlying periosteum was removed from the bone. A small craniotomy was made in the bone over the brainstem, and the dural tissue was carefully cleared to expose the brain. The cannula of the recording assembly was then lowered into the brain, until the tip of the cannula reached a position just dorsal of the vestibular nuclear complex. The assembly was attached to the skull using three inverted stainless steel T-bolts and dental acrylic surrounding the nylon cuffs at the end of each drive screw. Each animal was also implanted with a Delrin head stud, used to fix the head during experiments. This stud was positioned with the beak tilted ~12° downward, such that upright orientation corresponded on average to alignment of the horizontal semicircular canals with an earth-horizontal plane (Dickman, 1996). After surgery, the wound margin was sutured closed, and the craniotomy was kept clear of debris by a removable head cap.

Behavioral and neural recording. Behavioral procedures used in these experiments have been described previously (McArthur and Dickman, 2011). In brief, the animal was secured to a restraint arm mounted to a six degrees-of-freedom hydraulic motion platform (Rexroth-Bosch) using a minimal restraint that left the animal's wings, tail, and legs free to move (see Fig. 1*A*,*B*). The animal's head could be fixed to the restraint arm (using the head stud) or left free to move. Rotational head movements were monitored using a three-field AC magnetic coil system (Riverbend Instruments) mounted to the motion platform and a 3D coil assembly attached to the head stud. The head was centered within the field coils and relative to the axes of rotational motion (see below). Further, the position of the body holder was adjusted for each animal such that its at-rest, head-free head position (on average) was approximately the same as its position during head-fixed recordings. Tail movements were monitored using an infrared optical tracking system (Optotrak Certus, Northern Digital), and a 3D rigid body (~8 g) temporarily secured to the animal's tail.

Extracellular neural recordings were obtained using the chronically implanted microdrive assembly. The neural signal of each electrode was differentially amplified (using the cannula as reference) by a custom-made head stage connected to the microdrive with a flexible wire tether. Neural signals were filtered (300–5000 Hz) and amplified (1000×) by the head stage, then filtered (100 Hz-10 kHz) and amplified (10×) further and stored as digital waveforms (20 kHz sampling rate) using a programmable interface (Power1401, Cambridge Electronic Design) and commercial software (Spike2, Cambridge Electronic Design). Neural waveforms, behavioral data (head and tail movements), and accelerometer and rate sensor signals were monitored on-line and time-synced off-line for further analyses.

Motion stimuli. The motion platform was driven by computer and a programmable interface (Power1401, Cambridge Electronic Design), using custom scripts written for the interface environment (Spike2, Cambridge Electronic Design). Stimulus deliveries were monitored using a rate sensor and three-axis linear accelerometer mounted to the motion platform. Under head-fixed conditions, the *x*-, *y*-, and *z*-axes corresponded to the animal's naso-occipital, interaural, and dorsoventral axes, respectively. Positive rotations were right ear down, nose down, and leftward. Positive translations were forward, leftward, and upward. Sinusoidal rotations were delivered about the *x*- (roll), *y*- (pitch), and *z*- (yaw) axes at 0.25, 0.5 and 1 Hz and amplitudes of 5, 10, 15, and 20°/s peak angular velocity. Sinusoidal translations were delivered along the *x*- (fore–aft) and *y*- (left–right) axes at 0.5 Hz with a peak amplitude of 0.1G (1G = 9.8 m/s).

Experimental protocol. All experiments were performed in darkness. To test the effect of behavioral state on neural responses to motion, we delivered rotational and translational motion in the absence of airflow and during an airflow-simulated gliding flight condition. Flight-state simulation has been described previously in detail (McArthur and Dickman, 2011). In brief, airflow was delivered to the animal's frontal surface using a blower hose fixed to the motion platform. In the absence of airflow (Fig. 1*A*, default state), pigeons were relaxed in the sling with their tails lowered and their legs extended underneath their torsos. In the presence of airflow (Fig. 1*B*, flight state), pigeons tensed their wings, lifted their tails, and pulled their legs up underneath their tails. Trials were blocked by stimulus axis, frequency, and behavioral state (default or flight), and at least 60 s passed between blocks. Between blocks, the experimental room was briefly and dimly lit, and animals were monitored for alertness (by visual inspection of posture and spontaneous head movements) and for successful transitions in behavioral state.

At the beginning of an experiment, neural signal channels were monitored for single-unit action potentials, in both the presence and absence of airflow. All well isolated single units (as judged on-line by the experimenter) were subjected to a battery of test stimuli, comprised of *x*-, *y*-, and *z*-axis rotations (0.5 Hz, 10 or 15°/s) in which airflow was turned on mid-motion. Any single-unit neuron with a systematic cycle-by-cycle response to any axis of motion (in the presence or absence of airflow) was deemed motion sensitive and recorded during additional stimuli. Based on neural responses to test stimuli, the experimenter selected on-line the cardinal axis of maximum sensitivity, and this axis was the basis of the experimental protocol for that neuron. For example, a neuron with a strong response to *y*-axis rotation would be recorded during 0.25–1 Hz, 5–20°/s pitch rotations and 0.5 Hz, 0.1 G *x*- and *y*-axis translations, repeated in the presence and absence of airflow (default/flight states), performed under head-fixed and head-free conditions, assuming continuous single-unit isolation. All neurons that were classified as motion sensitive on-line (and could be reliably spike sorted; see below) were confirmed to be motion sensitive off-line (mean sensitivity >0.1 spikes/s per degree/s).

Recording location. Extracellular recordings were targeted to the lateral portion of the vestibular nuclear complex, based upon previously determined stereotaxic coordinates in pigeons (Dickman and Fang, 1996). Because the microdrive and cannula were chronically implanted, there was a single recording track per pigeon, through the left hemisphere. The locations of the recording tracks were confirmed by histology (Fig. 1*C*). After all experiments were completed, each animal received a lethal dose of sodium pentobarbital and underwent cardiac perfusion (2% glutaraldehyde, 1% paraformaldehyde). Fixed brain tissue was frozen, then sectioned (50 μm), mounted on slides, and counterstained with neutral red. Sections were viewed for electrode location using a Nikon Eclipse E600 microscope.

Neuronal classification. Neurons were classified into three groups, based on their spontaneous activity and responses to rotational stimuli. One group of neurons exhibited no spontaneous activity and was only sensitive to rotational motion during the flight state. These neurons were classified as "air-on" neurons. The second and third groups of cells both exhibited spontaneous activity and responded to rotation during both default and flight states. Of these, neurons that exhibited bursts and/or pauses in firing related to eye movements (as assessed by the experimenter during spontaneous saccades in the light) were classified as eye movement (EM) neurons. All other spontaneously active neurons were classified as non-eye movement (NEM) neurons.

Data analyses. All analyses were performed using custom scripts in Matlab (Mathworks). Head and tail movement signals were converted to rotation vectors in Cartesian coordinates, as described previously

(McArthur and Dickman, 2011). Action potentials were sorted off-line using commercial software implementation (Spike2, Cambridge Electronic Design) of semiautomated spike shape template matching, and any putative single units for which this procedure could not be reliably implemented (due to significant changes in spike shape across files or to a low signal-to-noise ratio) were discarded. Single-unit neural spike times were converted to instantaneous firing rates (IFRs). First, to quantify steady-state spontaneous firing rate during each behavioral context, 5 to 10 s segments of data were taken from prestimulus and poststimulus periods (head fixed only), and average firing rates [spikes per second (spk/s)] were computed for each trial. Data segments that contained transient head and/or tail movements (i.e., gaze saccades, tail lifts) were excluded, as were data segments containing bursts or pauses in firing rate (for EM neurons). To characterize transient changes in firing associated with transitions between behavioral contexts, segments of spontaneous firing (i.e., no whole-body motion stimuli) in which behavioral state transitions were triggered by changes in airflow were fit with an exponential decay function to the IFR data. Next, for each sinusoidal response, steady-state neuronal IFRs, as well as rate sensor and accelerometer signals, were fit with sine curves at the fundamental stimulus frequency using a least-squares minimization algorithm. The fitted curves were used to calculate the gain and phase values of the neural response, relative to the stimulus. For rotational stimuli, neural gains were expressed as the peak change in IFR (spk/s) relative to peak angular velocity (°/s), and phase values were expressed relative to peak positive angular velocity. Responses to translational stimuli were expressed relative to the apparent tilt—that is, the earth-horizontal axis rotation that would produce the equivalent linear acceleration stimulus in the head (McArthur and Dickman, 2008). For example, an *x*-axis (fore–aft) translation (0.5 Hz, 0.1G) would correspond to an apparent *y*-axis (pitch) tilt (0.5 Hz, ±6°, ~20°/s), allowing us to directly compare neural responses to these two stimuli where the linear acceleration stimulus to the animal was matched.

In addition to steady-state gain and phase, half-cycle spike counts were also used to analyze neural responses to motion. On each trial, the sinusoidal fit to the IFR data was used to cut the neural response into excitatory (+) and inhibitory (−) half-cycle segments. The number of spikes in each full half-segment was counted, and the mean + and − spike counts for that trial were computed. Although the IFR sinusoidal fit was used to establish half-cycle start times, the spike counts themselves were independent of response nonlinearities (i.e., IFR rectification) that could affect the gain values. Thus, when determining whether the magnitude of a neuron's response depended on behavioral state, statistical analyses were performed on both IFR gain and +/− spike counts.

All statistical analyses were performed using Statistica (Statsoft).

Cell-by-cell analyses. To determine whether a single neuron's response to rotation was state dependent, a Wilcoxon matched-pair test was performed, in which each pair of values (gain, phase, + or − spike count) were matched for stimulus axis (*x*/*y*/*z*), amplitude (5–20°/s), and frequency (0.25–1 Hz) but were recorded under different behavioral conditions (default/flight). A *t* test for dependent samples was used to determine whether spontaneous firing rate was state dependent.

Population analyses by category. To determine whether the rotational gains of a given neuronal category were dependent on velocity, frequency, and behavioral state, a factorial ANOVA was performed across cells in that category (air-on, EM, or NEM) using all available head-fixed data for the preferred cardinal axis of rotation of each unit, with behavioral state (default/flight) and either frequency or velocity as factors. To compare rotational responses under head-fixed and head-free conditions, IFR gains were subjected to an ANOVA with head-fixed/head-free and behavioral state as factors. To quantify the relationship between rotational and translational (apparent tilt) gains for each neuronal category, linear regressions were fit to the gain data (separately for each behavioral state) using a fitting algorithm that accounted for the use of two dependent variables by minimizing perpendicular errors and computing asymmetrical confidence intervals.

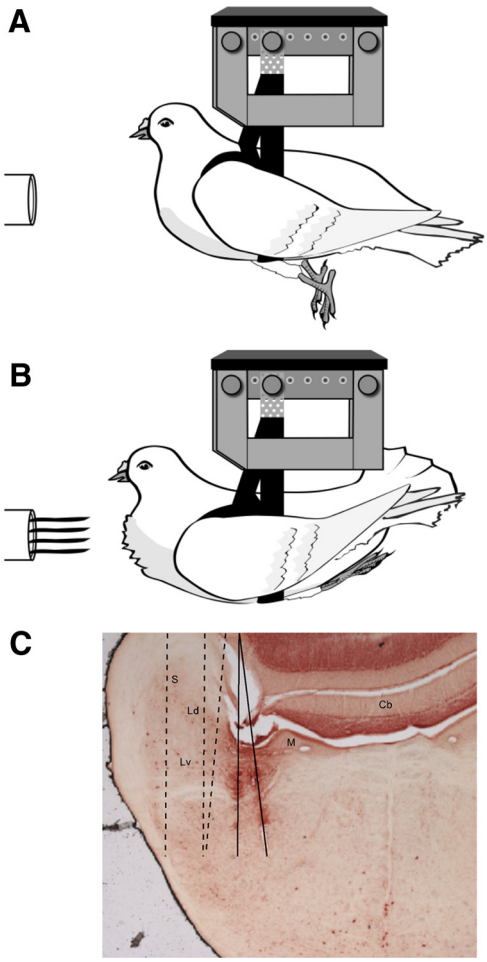

Figure 1. Frontal airflow triggers a change in a pigeon's behavioral state. ***A***, Default state (air-off). ***B***, Flight state (air-on). (Credit: Marcy Hartstein, MedPIC, Washington University School of Medicine, St. Louis, MO.) ***C***, Recording electrode tracks for the 10-wire electrode array penetrating through the vestibular nuclei of four birds. Solid lines indicate the track of one array that had split into two clusters of electrodes during the penetration. Dashed lines indicate the approximate tracks from three other animals, based on histological verification. Cb, Cerebellum; Ld, dorsal lateral vestibular nucleus; Lv, ventral lateral vestibular nucleus; M, medial vestibular nucleus; S, superior vestibular nucleus.

Results

Flight state and state-dependent vestibular reflexes

To characterize the effect of behavioral state on neural responses to motion, we used frontal airflow to simulate a gliding flight state in minimally restrained pigeons, signaled by a robust postural change including elevation of the tail and extension of the legs underneath the tail (Fig. 1, compare *A*, *B*). Single-unit neuronal activity was recorded from the VNC in the pigeon brainstem. We confirmed that birds implanted with chronic microdrives for neural recording still exhibited state-dependent vestibular behaviors, by recording their head and tail movements during experiments (Fig. 2, sample behavioral data). Indeed, as previously described for birds without microdrives (McArthur and Dickman, 2011), animals used in the current study increased the gain of their VCR during flight. Further, a strong compensatory tail response to pitch rotation was observed specifically during flight, with the appropriate temporal relationship to the rotational stimulus to contribute to stable body orientation during actual flight. Thus, the previously reported phenomenon of state-dependent vestibular processing was actively occurring during the neural recordings described in the current study.

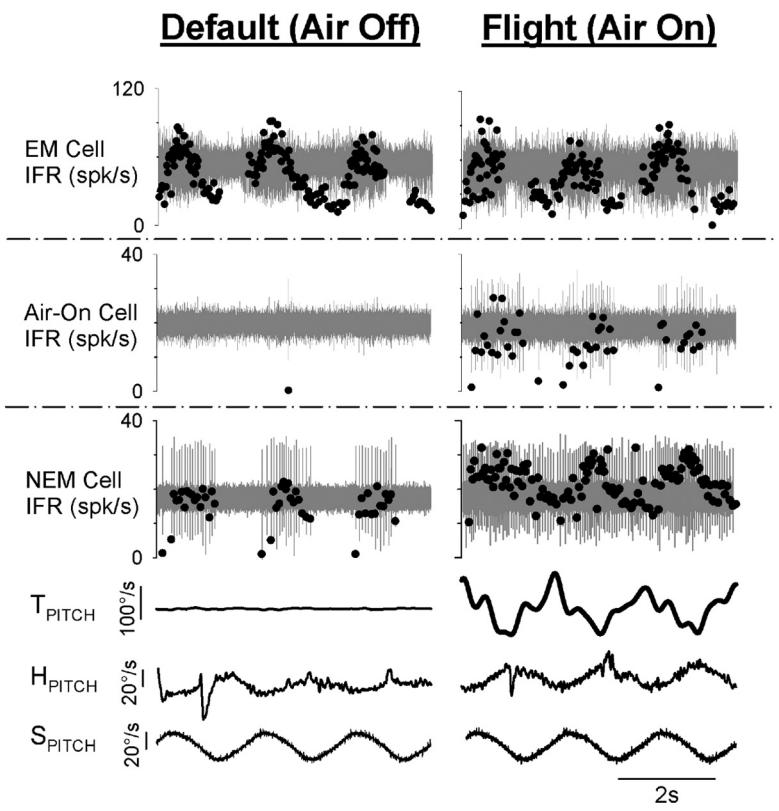

Figure 2. Sample behavioral and neuronal responses to rotational motion during two behavioral states: default state (left column) and simulated flight (right column). All data were recorded during *y*-axis (pitch) rotation (0.5 Hz, 20°/s). Representative EM (head-fixed), air-on (head-fixed), and NEM (head-free) neuronal responses are shown in the top, second, and third row panels, respectively. Stimulus angular velocity (S_{PITCH}), head-on-body velocity (H_{PITCH}), and tail-on-body velocity (T_{PITCH}) are shown in the bottom three panels and were recorded simultaneously with the NEM cell under head-free conditions. Neural waveforms are shown in gray, and corresponding IFRs are overlaid as black dots.

Reconstruction of recording electrode tracks (Fig. 1*C*) confirmed that the majority of the neurons included in this study were located in the LVN, while some medial vestibular nuclei and superior vestibular nuclei cells were also likely included. All well isolated single units that were sensitive to at least one cardinal axis of rotation (roll/pitch/yaw) during at least one behavioral state (default/flight) were analyzed further. Motion-sensitive neurons in the VNC ($n = 27$) were divided into three categories, based on qualitative observations regarding their spontaneous firing rates, rotation sensitivity, and correlations between their activity and behavior (Fig. 2). Most neurons fired action potentials spontaneously during at least one behavioral state. Of these, neurons that also showed bursts or pauses in their firing rates correlated with saccades were categorized as EM neurons ($n = 6$); the remaining spontaneously active neurons were categorized as NEM neurons ($n = 13$). Both EM and NEM neurons were rotation sensitive during both behavioral states. A third group of neurons ($n = 8$) was not spontaneously active during either behavioral state, nor were they rotation sensitive during the default state. However, during simulated flight, these neurons became sensitive to rotational motion and were thus categorized as air-on neurons. Both NEM and air-on neurons sometimes exhibited transient increases in firing rate correlated with sudden, large tail movements (data not shown). While neurons like the EM and NEM neurons analyzed here have been reported previously (Scudder and Fuchs, 1992), air-on neurons have not been previously described, to the best of our knowledge.

Spontaneous firing rate

NEM and EM neurons exhibited spontaneous firing rates ranging from 0 to 150 spk/s in the default state (Fig. 3*B*). For EM neurons, mean values of 38.3 spk/s and 60.0 spk/s were observed for the default and flight states, respectively. These values were generally higher than those observed for NEM neurons, where mean values of 15.6 spk/s (default) and 25.4 spk/s (flight) were observed. However, both EM and NEM neurons exhibited significantly higher firing rates during simulated flight (*t* test: NEM, $p < 0.05$ for 13/13 cells; EM, $p < 0.05$ for 5/6 cells) (Fig. 3*B*). The dynamics of the transitions between flight states are shown for a representative NEM neuron in Figure 3*A*. Upon the onset of airflow and the beginning of the flight state, there was an initial steep rise in firing rate, followed by an exponential decay ($\tau < 1$ s) to a sustained firing level that was higher than the original preairflow firing rate. When the airflow ended and the animal returned to its default state, the firing rate quickly decayed back to its original level ($\tau < 1$ s). This pattern of transition was consistent for all EM and NEM neurons.

Rotation response: gain and phase by category

The differences in cell groups and the effect of behavioral state are evident in the mean motion response curves shown in Figure 4*A*. During the default condition, only EM (Fig. 4*A*, green) and NEM (Fig. 4*A*, blue) neurons were sensitive to head-fixed rotations. However, air-on (Fig. 4*A*, red) neurons only responded to rotation specifically during flight. All three neuronal categories exhibited rotational gains that decreased with increasing stimulus peak velocity ($p < 0.002$, ANOVA). However, only air-on neuronal gains depended on stimulus frequency, tending to be higher during lower-frequency stimuli ($p = 0.02$, ANOVA). In no case was there a significant interaction between either stimulus velocity or frequency and the effect of behavioral state ($p > 0.7$, ANOVA). The largest state-dependent change in response was exhibited by the air-on neurons, each of which increased its gain from zero during the default state to values ranging from 0.1 to 1 during flight (Fig. 4*A*, filled vs open red symbols). When considered as a category, the NEM neurons also exhibited state-dependent rotational sensitivity ($p = 0.06$, ANOVA), though their gains tended to be lower during flight, while the EM cell population did not show significant state-dependent gains overall ($p > 0.9$, ANOVA). Further, for the subset of neurons ($n = 12$) recorded under both head-fixed and head-free conditions, the effect of state on neural gains was similar under both conditions ($p > 0.2$, ANOVA, state *x* head-fixed/free; data not shown).

The temporal relationship, or phase, between rotational stimuli and neural responses varied widely across the population (Fig. 4*B*), although some clustering was observed by cell category. Most EM cells (Fig. 4*B*, green) exhibited peak firing rates that were approximately in phase with the peak angular head velocity

(IFR phase = 0°). In contrast, most NEM (Fig. 4*B*, blue) cells fired approximately in phase with peak stimulus position (IFR phase = −90°). Air-on (Fig. 4*B*, red) cells were mixed; some had phases between stimulus position and velocity (−30° to −75°), and a few were closer to stimulus acceleration (90–135°). One cell from each group fired out of phase relative to peak angular velocity (IFR phase = −180°). Neither EM nor NEM cell populations exhibited a significant effect of frequency or velocity on phase ($p > 0.3$, ANOVA), and the effect on air-on neural phase was highly variable across neurons (data not shown). Further, the response phase of most EM and NEM neurons did not vary across behavioral states (Fig. 4*B*, filled vs open symbols in each row) (5/6 EM cells and 11/13 NEM cells with $p > 0.05$, Wilcoxon matched-pair test). Thus, we did not analyze response phase further.

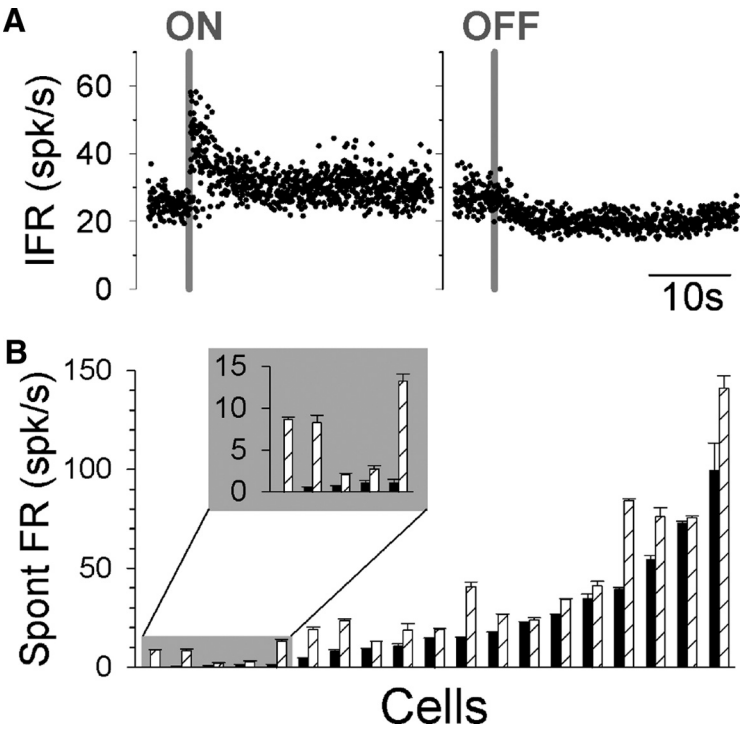

Figure 3. Spontaneous firing rates of NEM and EM neurons are state dependent. ***A***, Representative NEM neuron's activity during transitions from default to flight state (left) and from flight to default state (right). Gray lines indicate airflow onset (ON) and offset (OFF). ***B***, Mean (±SEM) spontaneous firing rates measured for each neuron during default (solid bars) and flight (hatched bars) states. A subset of neurons with the lowest spontaneous firing rates (inset) exhibited rectification during modulated firing in response to sinusoidal rotation. Spont, Spontaneous.

Rotation response: gain and spike counts cell by cell

The state dependence of air-on neurons was clearly homogeneous, in that every neuron exhibited the same state-specific rotation sensitivity during flight. However, when data were pooled across neurons in other categories, it was unclear whether behavioral state had a real effect on neural response and whether or not this effect was similar across neurons. To address this issue, we conducted a cell-by-cell comparison of NEM and EM cell IFR gains during default and flight states, matched by stimulus amplitude and frequency (Fig. 5*A*). The results indicated that approximately one-half of these neurons (Fig. 5*A*, blue) had lower rotational gains during flight ($p < 0.07$, Wilcoxon matched-pair test; 1/6 EM neurons, 9/13 NEM neurons). An additional two NEM neurons (Fig. 5*A*, red) responded with higher gains during flight ($p < 0.08$, Wilcoxon matched-pair test), and the remaining EM and NEM neurons (Fig. 5*A*, black) did not significantly change their gain as a function of behavioral state. Thus, cell-by-cell analyses were consistent with the trends observed for the population data, but there may be some real heterogeneity among neurons in the same category regarding the effect of state on rotational gains.

While the IFR gain provides one measure of a neuron's sensitivity to sinusoidal motion stimuli, this metric is derived from the depth of the modulation in firing rate (peak to trough) during the stimulus cycle around the mean firing rate (generally close to the value of the spontaneous firing rate). Thus, a neuron might exhibit higher activity during the flight state without changing its IFR gain value, if the difference in its peak and trough firing rates remains proportionally the same. Alternatively, a neuron with a low spontaneous firing rate during the default state could exhibit rectification during rotational motion, when the trough firing rate was driven to zero (Fig. 2, NEM neuron). However, during flight, the neuron's baseline firing rate would increase, and the IFR modulation would no longer rectify, thereby decreasing the proportional peak-trough modulation and decreasing its gain value. Although IFR gain serves as an important measure of neural sensitivity, neural information transmission may rely more upon absolute firing rate or spike density than on cyclical modulation. Thus, we next quantified the mean number of spikes fired by each neuron during its excitatory response to the sinusoidal rotation stimulus (Fig. 5*B*, + spike counts). While some neurons exhibited lower gains during the flight state, no neurons decreased the number of spikes they fired during an excitatory stimulus. On the contrary, approximately one-half of the population (Fig. 5*B*, red) had significantly higher excitatory spike counts during flight ($p < 0.06$, Wilcoxon matched-pair test; 3/6 EM neurons, 7/13 NEM neurons). In fact, some neurons exhibited both a lower gain and a higher excitatory spike count during flight. Thus, the effect of state on EM and NEM neurons, though somewhat heterogeneous across cells, may be best described as an increase in the number of spikes fired during an excitatory rotational stimulus, against a background of higher overall activity—similar to the observed increase in firing activity to rotation during flight observed for air-on neurons.

Response to rotation versus translation

Most EM and NEM neurons that were sensitive to pitch and roll rotation also responded during head-fixed horizontal linear translations (0.5 Hz, 0.1G) along the fore–aft axis, lateral axis, or both during both default and flight states. Most strikingly, the relative amplitude of rotational and translational responses was highly state dependent for the air-on neurons. As previously noted, air-on neurons responded to rotation only during flight. However, all air-on neurons did respond to translation during the default state. For example, the representative air-on neuron shown in Figure 6 responded to translation (Fig. 6*A*) during both default and flight states, but this cell only responded to rotation (Fig. 6*B*) during flight. Note that the rotational stimulus was an earth-horizontal pitch rotation about the animal's interaural axis

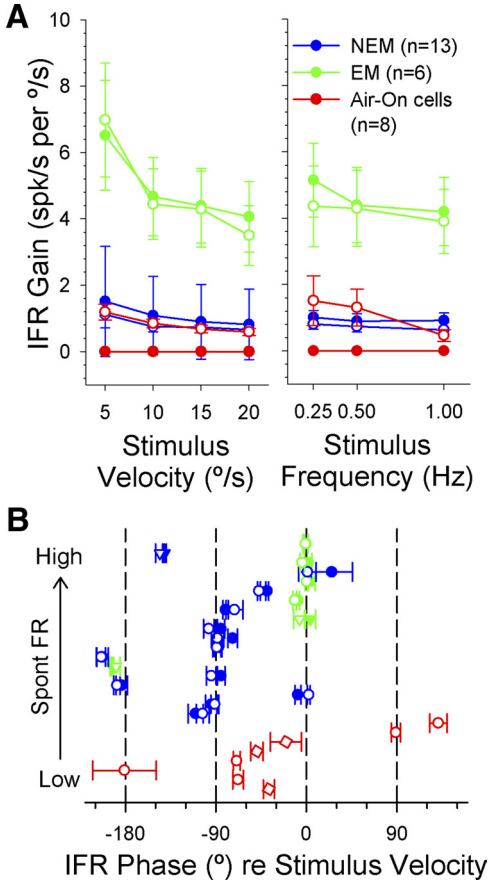

Figure 4. Neuronal responses to head-fixed preferred cardinal axis rotation during two behavioral states. ***A***, Mean (±SEM) IFR gain values for each neuronal category (air-on, red: $n = 8$; NEM, blue: $n = 13$; EM, green: $n = 6$) during default (solid symbols) and flight (open symbols) states, plotted as a function of stimulus frequency (15°/s peak) and peak velocity (0.5 Hz). ***B***, Mean (±SEM) IFR phase values for each neuron, color coded by neuronal category. Neurons are ordered bottom to top by increasing spontaneous firing rate, with air-on neurons (red) at bottom (with arbitrary within-group ordering), then NEM (blue) and EM (green) neurons (using same ordering as shown in Fig. 3*B*). Phases were recorded during head-fixed rotational motion about that neuron's preferred axis (square = *x*-axis, circle = *y*-axis, triangle = *z*-axis) during default (solid symbols) and flight (open symbols) states, averaged across stimulus frequency and velocity. Note that phase values of −90° and 0° correspond to responses that are in phase with stimulus angular position and velocity, respectively. Spont, Spontaneous.

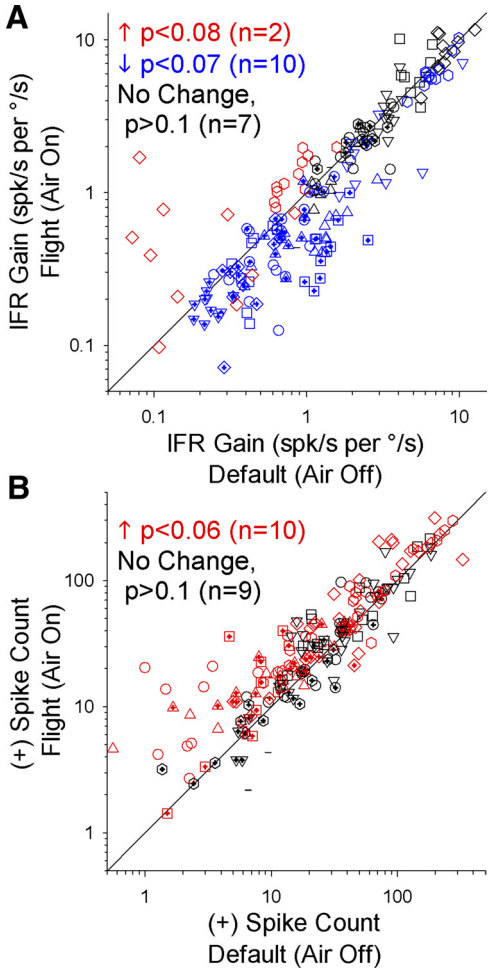

Figure 5. Comparison of gains and spike counts for NEM and EM neurons during default (air-off) and flight (air-on) states. All data were recorded during head-fixed rotational motion along a given neuron's preferred cardinal axis (*x*/*y*/*z*) of rotation. Each data point corresponds to a single neuron's response to a specific combination of stimulus velocity (5–20°/s) and frequency (0.25–1 Hz), presented in the presence and absence of airflow. Each symbol shape of a particular color corresponds to the available data for a single neuron, and symbol color indicates whether the neuron had a significantly higher value (red), lower value (blue), or no change in value (black) between behavioral states, based on the results of a Wilcoxon matched-pair test. ***A***, Gain values (spk/s per °/s) from steady-state sinusoidal fits to the IFR. ***B***, Mean + half-cycle spike counts.

(0.5 Hz, 20°/s). Due to reorientation of the head relative to gravity (±6°), the pitch stimulus also generated a sinusoidal linear acceleration along the animal's naso-occipital (fore–aft) axis (0.5 Hz, 0.1G). The combination of dynamic angular velocity and linear acceleration did not drive a response except during the flight state (Fig. 6*A*). However, linear acceleration alone (of the same frequency and amplitude) during translation was sufficient to drive a response during both default and flight states during translation (Fig. 6*B*). All air-on neurons exhibited this pattern: rotation responses were flight specific, while translation responses could be evoked during both behavioral states. These data are summarized and compared with the results for EM and NEM neurons in Figure 6*C*. Responses to translation are expressed relative to the equivalent rotational velocity (see Materials and Methods) to compare the relative strength of each response during head rotation relative to gravity. While air-on neurons (Fig. 6*C*, red) showed a clear preference for translation during the default state, most NEM neurons (Fig. 6*C*, blue) exhibited similar gains for tilt and translation across the two behavioral states, with the exception of a single outlying neuron that showed a preference for tilt (Fig. 6*C*, gray box; includes data for a single neuron recorded during two axes of stimulation, indicated by different symbol shapes). This observation was supported by linear regressions through the NEM cell data. Excluding the outlier, linear regressions relating NEM cell gain values during rotation and translation were highly significant ($p < 0.001$) for both default ($r = 0.96$) and flight ($r = 0.89$) states, with slopes that were not statistically distinguishable from unity (default: slope = 0.90, 95% CI = 0.66, 1.25; flight: slope = 1.04, 95% CI = 0.68, 1.585). Thus, a state-specific preferential response to translation over rotation appears to be restricted to the population of air-on neurons.

Discussion

Our objective was to provide an initial characterization of state-dependent responses in the vestibular nuclear complex. Behavioral state had an effect on the activity of all vestibular motion-sensitive neurons observed, though the nature of this effect varied cell by cell. Spontaneous firing rates were higher during flight for both EM and NEM neurons. While the number of excitatory

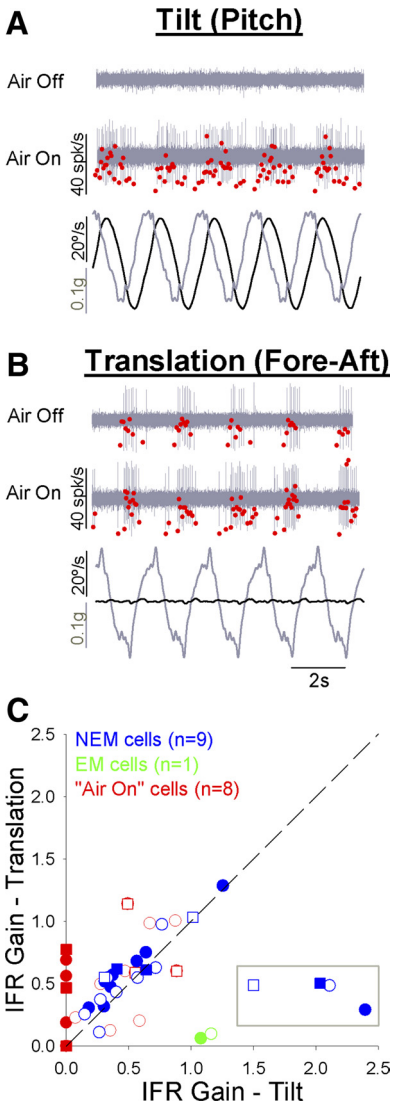

Figure 6. Comparison of responses to rotational (tilt) and translational (apparent tilt) stimuli. ***A***, ***B***, Representative air-on neuron response to head-fixed 0.5 Hz tilt (***A***, pitch, 20°/s) and translation (***B***, fore–aft, 0.1G). Stimulus traces (bottom of each panel) show angular velocity (black) and linear acceleration (gray) components of each stimulus. Neural responses are shown for the same air-on neuron during default (Air Off) and flight (Air On) states. Neural waveforms are shown in gray, and the corresponding IFR values are overlaid in red. ***C***, Comparison of rotational and translational gain values across neurons, expressed relative to apparent tilt velocity (see Materials and Methods). Data are plotted for all air-on (red, $n = 8$), EM (green, $n = 1$), and NEM (blue, $n = 9$) neurons for which data were available, and all appropriate data from a single neuron were included (responses to either one or two motion axes per unit). Circles, Pitch rotation/fore–aft translation; squares, roll rotation/lateral translation. Data points inside of the gray box (***C***) belong to a single NEM neuron identified as an outlier (see Results).

spikes fired by EM and NEM neurons in response to rotational stimuli tended to be higher during flight, the air-on neurons exhibited the most dramatic state-dependent responses. Air-on neurons responded to translation during both behavioral states; however, these cells responded to rotation only during flight. These results provide insight into the underlying substrates for previously reported state-dependent vestibular behaviors in birds (McArthur and Dickman, 2011) and contribute to our general understanding of state-dependent neural processing.

State-dependent neural activity

One of the primary findings in the present study was the effect of state on the spontaneous firing rates of vestibular neurons. The transition from the default state into simulated flight dramatically increased the firing rate of all EM and NEM neurons, reaching the higher steady-state firing rate within the first few seconds following airflow onset. Others have observed facilitation of spontaneous activity in vestibulospinal LVN neurons in mammals, related to limb stimulation and simulated locomotion (Wilson et al., 1967; Orlovsky, 1972; Marlinsky, 1992). Facilitation of spontaneous neuronal activity has also been observed during simulated flight in flies for visual neurons driving optomotor responses (Longden and Krapp, 2009; Maimon et al., 2010). The flight-related increase in baseline activity enhanced the dynamic range of some neurons by bringing their modulated firing rates out of inhibitory rectification. The flight state might thus improve motion information fidelity by increasing the size of the population that encodes the entire movement profile (Longden and Krapp, 2009).

State-dependent responses to motion

In a previous study, we demonstrated that vestibular eye (VOR) and head (VCR) responses increased in gain during simulated flight (McArthur and Dickman, 2011). We predicted that vestibular neurons would exhibit similar gain increases during flight, providing the substrate for state-dependent facilitation of behavior. Instead, many vestibular EM and NEM neurons had modestly lower gains during flight, though this occurred against a background of higher activity overall. Only air-on neurons significantly increased their sensory gains during flight. These cells responded to translation across behavioral states, but their sensitivity to rotation was state specific and occurred only during flight. The activity of these air-on neurons would be consistent with state-specific gating or facilitation of their rotational inputs. To the best of our knowledge, state-specific vestibular neurons, like the air-on cells described here, have not been previously reported. We speculate that these neurons were Deiters' cells, a group of vestibulospinal neurons in the dorsal LVN that do not receive primary vestibular afferent input, exhibit low spontaneous activity, and have highly nonlinear responses to stimulation (Ito, 1972; Sun et al., 2002; Uno et al., 2003; Straka et al., 2005). What has been shown is that many vestibular neurons are modulated by the motion context, as with the attenuation of motion responses during active gaze shifts (Roy and Cullen, 1998; McCrea et al., 1999). Further, simulated locomotion can modulate vestibular sensitivity of neurons in the LVN (Orlovsky and Pavlova, 1972; Marlinsky, 1992). State-dependent facilitation of sensory sensitivity has also been demonstrated for fly visual neurons during walking (Chiappe et al., 2010) and flying (Longden and Krapp, 2009; Maimon et al., 2010; Rosner et al., 2010).

Neurons and state-dependent behavior

Several observations support the suggestion that air-on cells drive state-specific tail responses during flight. First, transient bursts of activity from some of these cells appeared to be correlated in time with strong, transient tail movements, likely representing either motor signals or proprioceptive feedback from tail muscles relayed by spinovestibular projections (Pompeiano, 1972). Also, though phase values varied across neurons, most air-on cells had peak responses that were nearly in phase with peak stimulus angular position (−90°), matching the phase of state-specific tail responses (McArthur and Dickman, 2011). Further, tail responses were apparent during pitch and roll rotation but not during yaw (McArthur and Dickman, 2011); similarly, the air-on neurons preferred pitch or roll rotation and responded minimally during yaw. The air-on neurons were not the only neurons

to exhibit these additional properties relating them to the tail response. In fact, many of the moderately active NEM neurons also responded in phase with stimulus position, preferred pitch and roll rotations, and modulated their firing rate with tail movements. Whether these neurons are also related to postural responses is unknown; however, NEM cells in other species have often been associated with vestibulospinal pathways (McCrea et al., 1999; Boyle, 2001; Sadeghi et al., 2009).

Since most EM and NEM cells exhibited modestly lower gain values during flight, what is driving the flight-related increase in VOR and VCR gains? One could speculate that the increase in behavioral gains is driven by the increased bidirectional signaling and greater number of neurons responding to the entire motion profile during flight, due to bilateral vestibular projections that converge onto motor neurons in the spinal cord (Rabin, 1975a,b). Alternatively, we observed higher excitatory spike counts during flight, carried by higher overall activity. Thus, it is possible that EM and NEM neurons drive higher behavioral gains through absolute firing rate and temporal summation, rather than the depth of modulation (gain) in the neural response. Finally, it is possible that the observed changes in neuronal activity and behavior might be mediated in parallel by the same central signal related to behavioral state but remain otherwise independent of one another, possibly through state-dependent modulation of reticulospinal pathways (Wilson and Peterson, 1981).

Possible mechanisms of state-dependent neuronal modulation

What is the nature of the central signal that drives neural and behavioral state dependence? We believe that the vestibular state-dependent processing shown here could be derived from modulations in cellular excitability. Each neuron would lie somewhere along a continuum of baseline excitability in the default state, with air-on, NEM, and EM neurons being of low, moderate, and high excitability, respectively. The transition into flight would shift the neuronal population toward higher excitability. For example, during the default state, the rotational input to air-on neurons is insufficient to exceed spiking threshold. However, during flight, rotation becomes an effective stimulus for air-on neurons against a background of increased excitability. Similarly, both NEM and EM neurons increase their excitability during flight, reflected in higher firing rates that no longer rectify during sinusoidal modulation.

Others have demonstrated changes in intrinsic cellular excitability in the vestibular nuclei as occur following periods of inhibition (Nelson et al., 2003) and during vestibular compensation (for review, see Straka et al., 2005). Further, there are at least two key synaptic inputs to LVN neurons that could strongly influence their excitability in a state-dependent manner. The locus ceruleus (LC) sends noradrenergic projections to the vestibular nuclei, particularly to Deiters' cells in dorsal LVN (Schuerger and Balaban, 1993) where norepinephrine application increases neuronal excitability (Yamamoto, 1967; Kirsten and Sharma, 1976). In fact, the invertebrate adrenergic homolog octopamine increases visuomotor neuronal excitability in flies and is used to simulate the flight state (Longden and Krapp, 2009) (for review, see Roeder, 2005). Noradrenergic LC projections might, as a result, similarly signal the flight state in pigeons and increase LVN neuronal excitability, which is associated with the switch to an active-locomotor condition. However, the time course of norepinephrine's action in LVN (~30–60 s) was longer than that observed for state-dependent changes evoked by airflow. An alternative mechanism might be the state-dependent modulation of tonic GABAergic inhibition from Purkinje cells in cerebellar cortex. Application of GABA causes strong, rapid hyperpolarization of the membrane potential and decreased excitability in LVN neurons (Obata et al., 1967). Further, LVN neurons receive a balance of monosynaptic cerebellar inputs, with tonic inhibition from the cortex (Ito and Yoshida, 1966; Ito et al., 1968) and excitation from the deep nuclei (Ito, 1972). Though previous work has been done primarily in mammals, there are consistent anatomical projections from cerebellar cortex and the medial cerebellar nucleus in pigeons (Arends and Zeigler, 1991ab). The cerebellar cortex receives convergent multisensory inputs that could determine the bird's behavioral state (Shelhamer and Zee, 2003; Manzoni, 2005, 2007) and modulate the balance of cerebellar excitation and inhibition accordingly, thus implementing state-dependent excitability of LVN neurons and possibly other neuronal populations driving the eye, head, and tail. Indeed, this balance of cerebellar inputs might provide a common mechanism across species for modifying the excitability of sensorimotor populations based on a multitude of factors related to behavioral state.

References

Arends JJ, Zeigler HP (1991a) Organization of the cerebellum in the pigeon (Columba livia): I. Corticonuclear and corticovestibular connections. J Comp Neurol 306:221–244.

Arends JJ, Zeigler HP (1991b) Organization of the cerebellum in the pigeon (Columba livia): II. Projections of the cerebellar nuclei. J Comp Neurol 306:245–272.

Bilo D (1992) Optocollic reflexes and neck flexion-related activity of flight control muscles in the airflow-stimulated pigeon. In: The head-neck sensory motor system (Berthoz A, Graf WM, Vidal PP, eds), pp 96–100. New York: Oxford UP.

Bilo D (1994) Course control during flight. In: Perception and motor control in birds (Davies MNO, Green PR, eds), pp 227–247. Berlin: Springer.

Bilo D, Bilo A (1978) Wind stimuli control vestibular and optokinetic reflexes in the pigeon. Naturwissenschaften 65:161–162.

Bilo D, Bilo A (1983) Neck flexion related activity of flight control muscles in the flow-stimulated pigeon. J Comp Physiol A Neuroethol Sens Neural Behav Physiol 153:111–122.

Boyle R (2001) Vestibulospinal control of reflex and voluntary head movement. Ann NY Acad Sci 942:364–380.

Brown RHJ (1963) The flight of birds. Biol Rev 38:460–489.

Chiappe ME, Seelig JD, Reiser MB, Jayaraman V (2010) Walking modulates speed sensitivity in Drosophila motion vision. Curr Biol 20:1470–1475.

Cullen KE, Chen-Huang C, McCrea RA (1993) Firing behavior of brain stem neurons during voluntary cancellation of the horizontal vestibulo-ocular reflex. II. Eye movement related neurons. J Neurophysiol 70:844–856.

Dickman JD (1996) Spatial orientation of semicircular canals and afferent sensitivity vectors in pigeons. Exp Brain Res 111:8–20.

Dickman JD, Fang Q (1996) Differential central projections of vestibular afferents in pigeons. J Comp Neurol 367:110–131.

Erichsen JT, Hodos W, Evinger C, Bessette BB, Phillips SJ (1989) Head orientation in pigeons: postural, locomotor and visual determinants. Brain Behav Evol 33:268–278.

Gioanni H, Sansonetti A (1999) Characteristics of slow and fast phases of the optocollic reflex (OCR) in head free pigeons (Columba livia): influence of flight behaviour. Eur J Neurosci 11:155–166.

Gioanni H, Sansonetti A (2000) Role of basal ganglia and ectostriatum in the context-dependent properties of the optocollic reflex (OCR) in the pigeon (Columba livia): a lesion study. Eur J Neurosci 12:1055–1070.

Ito M (1972) Cerebellar control of the vestibular neurons: physiology and pharmacology. Prog Brain Res 37:377–390.

Ito M, Yoshida M (1966) The origin of cerebellar-induced inhibition of Deiters neurons. I. Monosynaptic initiation of the inhibitory postsynaptic potentials. Exp Brain Res 2:330–349.

Ito M, Kawai N, Udo M, Sato N (1968) Cerebellar-evoked disinhibition in dorsal Deiters neurons. Exp Brain Res 6:247–264.

Kirsten EB, Sharma JN (1976) Characteristics and response differences to iontophoretically applied norepinephrine, D-amphetamine and acetyl-

choline on neurons in the medial and lateral vestibular nuclei of the cat. Brain Res 112:77–90.
Kubie JL (1984) A driveable bundle of microwires for collecting single-unit data from freely-moving rats. Physiol Behav 32:115–118.
Lisberger SG, Pavelko TA, Broussard DM (1994) Neural basis for motor learning in the vestibuloocular reflex of primates. I. Changes in the responses of brain stem neurons. J Neurophysiol 72:928–953.
Longden KD, Krapp HG (2009) State-dependent performance of optic-flow processing interneurons. J Neurophysiol 102:3606–3618.
Maimon G, Straw AD, Dickinson MH (2010) Active flight increases the gain of visual motion processing in Drosophila. Nat Neurosci 13:393–399.
Manzoni D (2005) The cerebellum may implement the appropriate coupling of sensory inputs and motor responses: evidence from vestibular physiology. Cerebellum 4:178–188.
Manzoni D (2007) The cerebellum and sensorimotor coupling: looking at the problem from the perspective of vestibular reflexes. Cerebellum 6:24–37.
Marlinsky VV (1992) Activity of lateral vestibular nucleus neurons during locomotion in the decerebrate guinea pig. Exp Brain Res 90:583–588.
Maurice M, Gioanni H (2004a) Eye-neck coupling during optokinetic responses in head-fixed pigeons (Columba livia): influence of the flying behaviour. Neuroscience 125:521–531.
Maurice M, Gioanni H (2004b) Role of the cervico-ocular reflex in the "flying" pigeon: interactions with the optokinetic reflex. Vis Neurosci 21:167–180.
McArthur KL, Dickman JD (2008) Canal and otolith contributions to compensatory tilt responses in pigeons. J Neurophysiol 100:1488–1497.
McArthur KL, Dickman JD (2011) State-dependent sensorimotor processing: gaze and posture stability during simulated flight in birds. J Neurophysiol 105:1689–1700.
McCrea RA, Gdowski GT, Boyle R, Belton T (1999) Firing behavior of vestibular neurons during active and passive head movements: vestibulospinal and other non-eye-movement related neurons. J Neurophysiol 82:416–428.
Nelson AB, Krispel CM, Sekirnjak C, du Lac S (2003) Long-lasting increases in intrinsic excitability triggered by inhibition. Neuron 40:609–620.
Obata K, Ito M, Ochi R, Sato N (1967) Pharmacological properties of the postsynaptic inhibition by Purkinje cell axons and the action of γ-aminobutyric acid on Deiters neurons. Exp Brain Res 4:43–57.
Orlovsky GN (1972) Activity of vestibulospinal neurons during locomotion. Brain Res 46:85–98.
Orlovsky GN, Pavlova GA (1972) Response of Deiters' neurons to tilt during locomotion. Brain Res 42:212–214.
Pompeiano O (1972) Spinovestibular relations: anatomical and physiological aspects. Prog Brain Res 37:263–296.
Precht W (1979) Vestibular mechanisms. Annu Rev Neurosci 2:265–289.
Rabin A (1973) Effects of stimulation of the vestibular labyrinth on intracellular responses of spinal motoneurons in the pigeon. Brain Res 62:231–236.
Rabin A (1974) Monosynaptic excitation and inhibition of spinal motoneurons by supraspinal structures in the pigeon. Brain Behav Evol 10:236–243.
Rabin A (1975a) Labyrinthine and vestibulospinal effects on spinal motoneurons in the pigeon. Exp Brain Res 22:431–448.
Rabin A (1975b) Electrophysiology of spinal motoneurons in the pigeon. Brain Res 84:351–356.
Roeder T (2005) Tyramine and octopamine: ruling behavior and metabolism. Annu Rev Entomol 50:447–477.
Rosner R, Egelhaaf M, Warzecha AK (2010) Behavioural state affects motion-sensitive neurons in the fly visual system. J Exp Biol 213:331–338.
Roy JE, Cullen KE (1998) A neural correlate for vestibulo-ocular reflex suppression during voluntary eye-head gaze shifts. Nat Neurosci 1:404–410.
Roy JE, Cullen KE (2002) Vestibuloocular reflex signal modulation during voluntary and passive head movements. J Neurophysiol 87:2337–2357.
Roy JE, Cullen KE (2004) Dissociating self-generated from passively applied head motion: neural mechanisms in the vestibular nuclei. J Neurosci 24:2102–2111.
Sadeghi SG, Mitchell DE, Cullen KE (2009) Different neural strategies for multimodal integration: comparison of two macaque monkey species. Exp Brain Res 195:45–57.
Schuerger RJ, Balaban CD (1993) Immunohistochemical demonstration of regionally selective projections from locus coeruleus to the vestibular nuclei in rats. Exp Brain Res 92:351–359.
Scudder CA, Fuchs AF (1992) Physiological and behavioral identification of vestibular nucleus neurons mediating the horizontal vestibuloocular reflex in trained rhesus monkey. J Neurophysiol 68:244–264.
Shelhamer M, Zee DS (2003) Context-specific adaptation and its significance for neurovestibular problems of space flight. J Vestib Res 13:345–362.
Straka H, Vibert N, Vidal PP, Moore LE, Dutia MB (2005) Intrinsic membrane properties of vertebrate vestibular neurons: function, development and plasticity. Prog Neurobiol 76:349–392.
Sun Y, Waller HJ, Godfrey DA, Rubin AM (2002) Spontaneous activity in rat vestibular nuclei in brain slices and effects of acetylcholine agonists and antagonists. Brain Res 934:58–68.
Taube JS, Muller RU, Ranck JB Jr (1990) Head-direction cells recorded from the postsubiculum in freely moving rats. I. Description and quantitative analysis. J Neurosci 10:420–435.
Uno A, Idoux E, Beraneck M, Vidal PP, Moore LE, Wilson VJ, Vibert N (2003) Static and dynamic membrane properties of lateral vestibular nucleus neurons in guinea pig brain stem slices. J Neurophysiol 90:1689–1703.
Warrick DR, Bundle MW, Dial KP (2002) Bird maneuvering flight: blurred bodies, clear heads. Integr Comp Biol 42:141–148.
Wilson VJ, Peterson BW (1981) Vestibulospinal and reticulospinal systems. In: Handbook of neurophysiology (Brooks VB, ed), pp 667–702. Bethesda, MD: American Physiological Society.
Wilson VJ, Kato M, Peterson BW, Wylie RM (1967) A single-unit analysis of the organization of Deiters' nucleus. J Neurophysiol 30:603–619.
Yamamoto C (1967) Pharmacologic studies of norepinephrine, acetylcholine and related compounds on neurons in Deiters' nucleus and the cerebellum. J Pharmacol Exp Ther 156:39–47.